Globally minimal surfaces by continuous maximal flows

Ben Appleton and Hugues Talbot

Abstract

In this paper we consider the problem of computing globally minimal continuous curves and surfaces for image segmentation and 3D reconstruction. This is solved using a maximal flow approach expressed as a PDE model. Previously proposed techniques yield either grid-biased solutions (graph-based approaches) or sub-optimal solutions (active contours and surfaces).

The proposed algorithm simulates the flow of an ideal fluid with a spatially varying velocity constraint derived from image data. A proof is given that the algorithm gives the globally maximal flow at convergence, along with an implementation scheme. The globally minimal surface may be obtained trivially from its output.

The new algorithm is applied to segmentation in 2D and 3D medical images and to 3D reconstruction from a stereo image pair. The results in 2D agree remarkably well with an existing planar minimal contour algorithm and the results in 3D segmentation and reconstruction demonstrate that the new algorithm is free from grid bias.

I. Introduction

Geometric optimisation techniques have been applied with great success to image segmentation and to stereo reconstruction. These techniques deal with the computation of curves, surfaces and partitionings which are optimal according to a measure dictated by the application domain. This measure may be designed ad-hoc or derived from a statistical model of the problem domain. Geometric optimisation has the distinct advantage over many other analysis techniques that practitioners must simply define an appropriate measure of goodness (objective function) and then optimise accordingly.

Geometric optimisation techniques include on the one hand active contour methods such as snakes [1], level sets [2], [3] and geodesic active contours [4], [5]; and on the other hand graph-theoretic methods such as shortest paths [6] and minimal cuts [7].

Active contour methods typically evolve an initial curve or surface via a gradient descent flow toward a locally minimal solution. Unfortunately in practice these methods are highly dependent on their initialisation and become stuck in local minima due to irrelevant features and image noise. Numerous ad-hoc schemes have been introduced in an attempt to increase their robustness, including artifical terms driving the surface toward deeper local minima and multiscale approaches which aim to track significant features through the image scales [8], [9]. Nonetheless active contours often require additional user interaction, limiting their effectiveness for many image analysis problems. Level set methods are introduced in [3].

Graph-theoretic methods have long enjoyed success in image analysis, particularly in 3D reconstruction. Stereo matching was first cast as a shortest path problem in the mid 1980's by Ohta and Kanade [10] and independently by Lloyd [11]. The approach is similar in current research [12], where the path through the correlation matrix of maximum sum is obtained. In recent years minimum cuts have also been applied to stereo matching yielding improved spatial consistency at the cost of additional computation [13]. These methods have been successfully applied to image segmentation in addition. In [14], Bamford and Lovell segment cell nucleii by computing a shortest path over a radial trellis centred on the nucleus. Many graph-theoretic methods enjoy the guarantee of an optimal solution according to their objective function, but suffer from significant discretisation artifacts exhibited as a preference for travel along the principle grid directions. An excellent introduction to graph-theoretic algorithms is Sedgewick's book [15].

Ideally geometric optimisation methods used in image analysis should be free of these problems, being both isotropic and optimal. In recent years several advances have been made extending optimal methods from discrete graphs to continuous spaces. Dijkstra's classic shortest path algorithm [6] was extended by Tsitsiklis [16] and by Sethian [17] to computing minimal geodesics and continuous distance functions. These have found broad application to optimal control, wave propagation and computer vision. The problem of continuous graph cuts has also received some attention. Hu described a method for approximating continuous minimal surfaces by a cut in a vertex weighted graph [23]. Boykov and Kolmogorov have recently proposed a method for computing edge weights which approximate continuous graph cuts, toward the goal of computing globally minimal surfaces for segmentation and stereo vision [24].

In this paper we present an algorithm to compute globally minimal curves, surfaces and

partitionings in arbitrary Riemannian spaces. *Structure of paper* ...

II. Geodesic Active Contours and Surfaces

Geodesic Active Contours and Surfaces were introduced by Caselles et. al. [4], [5] for segmentation in 2D and 3D images. They are manifolds of co-dimension one which minimise the integral:

$$E\left[S\right] = \int_S g(S) \mathrm{d}S. \tag{1}$$

$E[S]$ is defined as the energy of the surface S. In object segmentation $g : I\!R^N \rightarrow I\!R^+$ is typically a decreasing function of edge strength. Caselles et. al. proposed the following formula,

$$g = \frac{1}{1 + |\nabla G_\sigma \star I|^p} + \varepsilon. \tag{2}$$

Here $p = 1$ or 2 and $\varepsilon > 0$ is a surface area penalty term used to regularise the minimal surface. For such a metric with positive uniform lower bound Caselles et. al. showed that all local minima are smooth surfaces. The metric's role is to encapsulate local knowledge derived from the image. It may also be derived from a statistical model of the image *LIT REVIEW*.

Geodesic Active Contours and Surfaces evolve an initial surface via a gradient descent flow toward a local minima of the energy functional. We may derive the gradient descent flow by variational calculus, giving the Euler-Lagrange equation:

$$\frac{\partial S}{\partial t} = \left(g\kappa - \nabla g \cdot \vec{N} \right) \vec{N}. \tag{3}$$

Here κ is the mean curvature and $\vec{N}$ the surface normal.

Surface evolution may be implemented using a level set embedding due to Osher and Sethian [2]. For a function $\phi : I\!R^N \rightarrow I\!R$ whose zero level set is $S = \{\vec{x} \,|\phi(\vec{x}) = 0\}$, we may evolve ϕ so as to implement the gradient descent flow of Equation 3:

$$\frac{\partial \phi}{\partial t} = -(g\kappa - \nabla g \cdot \vec{N}) \left|\nabla \phi\right|.$$

A fast implicit update scheme has also been presented by Goldenberg et. al. [18]. Unfortunately as pointed out earlier these gradient descent flows usually converge to local minima.

III. Weighted graphs and Riemannian spaces

A number of geometric optimisation techniques have been proposed for computer vision based on discrete graphs [14], [13] and later continuous Riemannian spaces [19], [20]. Here we review the basic theory and definitions of these closely related frameworks.

A. Minimal Paths and Geodesics

A graph G is a pair (V, E) consisting of a vertex set V and an edge set $E \subseteq V \times V$. Vertices may be interpreted as points while edges are lines connecting pairs of points. A weighted graph includes vertex costs $C_V : V \to \mathbb{R}$ and edge costs $C_E : E \to \mathbb{R}$. In this paper we consider only positive cost functions.

A simple path P is defined as a sequence of unique vertices, while a cycle has equal endpoints so as to form a loop. The length L of a path P is the sum of vertex and edge costs along the path,

$$L[P] = \sum_{v \in P} C_V(v) + \sum_{e \in P} C_E(e).$$

The length of a cycle is defined analogously.

A path between two points s and t is a minimal or shortest path if there exists no connected path of lower length. Such paths may be computed using Dijkstra's shortest path algorithm [6], which first computes the distance function of each vertex from s before backtracking from t to s.

A Riemannian space R is the continuous equivalent of a weighted graph. It consists of a N-manifold Ω and an associated metric $g : \Omega \to \mathbb{R}$. Here we consider only positive scalar metrics $g \in \mathbb{R}^+$. A simple curve in a Riemannian space is a 1-manifold embedded in Ω which does not pass through itself. A curve C with parameter s in the range $[a, b]$ has length

$$L[C] = \int_a^b g(C(s)) \left| \frac{\partial C}{\partial s} \right| \mathrm{d}s.$$

A simple curve between two points s and t is a minimal geodesic if there exists no such curve of lower length. Minimal geodesics may be computed using Sethian's Fast Marching Method [17], which first computes a distance function from s by wavefront propagation before backtracking by gradient descent from t to s.

B. Minimal Cuts and Minimal Surfaces

A partitioning of a graph G decomposes its vertex set into a collection $\Gamma_G = \{V_1, V_2, \ldots\}$ of disjoint subsets:

$$\bigcup_{V_i \in \Gamma_G} V_i = V, \quad V_i \cap V_j = \emptyset \quad \text{for} \quad i \neq j$$

To each partition Γ_G we associate a cost $C(\Gamma_G)$ which is the total cost of the edges whose endpoints lie in different partitions.

$$C\left(\Gamma_G\right) = \sum_{e \in E^*} C_E\left(e\right)$$

Here the *cut* $E^* \subseteq E$ denotes the set of edges crossing the partition. The s-t minimal cut problem seeks the partitioning of minimal cost such that the disjoint vertex sets $s, t \subseteq V$ lie in different partitions. A good introduction to algorithms solving this problem is Sedgewick's book [15].

A partitioning of a Riemannian space R decomposes the space into a collection $\Gamma_R = \{\Omega_1, \Omega_2, \ldots\}$ of compact subsets whose pairwise intersection has zero Lebesgue measure:

$$\bigcup_{\Omega_i \in \Gamma_R} \Omega_i = \Omega, \quad \otimes_\rangle \cap \otimes_| = 0 \quad \text{for} \quad i \neq j.$$

Similarly to the discrete case, to each partition Γ_R we associate a cost $C(\Gamma_R)$ which is the integral of the metric g over the partition surfaces $\partial\Omega_i$,

$$C\left(\Gamma_R\right) = \frac{1}{2} \sum_{\Omega_i \in \Gamma_R} \oint_{\partial\Omega_i} g \mathrm{d}(\partial\Omega_i).$$

The potentially confusing term $d(\partial\Omega_i)$ denotes an infinitesimal component of the partition surface $\partial\Omega_i$.

In this continuous case, the s-t minimal cut problem seeks the partition Γ_R of minimal total cost such that the point sets $s, t \subseteq \Omega$ fall in different partitions. To the author's best knowledge this paper is the first to present an exact solution to the continuous minimal surface problem in the general case.

C. Maximal Flows

Let G be a graph with edge costs C_E now reinterpreted as *capacities*. A flow $F_G : E \to I\!R$ from a *source* $s \subseteq V$ to a *sink* $t \subseteq V$ has the following properties:

- Conservation of flow: The total (signed) flow in and out of any vertex is zero.
- Capacity constraint: The flow along any edge is less than or equal to its capacity: $\forall e \in E, \quad F\left(e\right) \leq C_E\left(e\right)$.

An edge along which the flow is equal to the capacity is decribed as *saturated*. In this and all future formulations, we implicitly add a directed edge connecting $t \to s$ of infinite capacity to conserve flow uniformly throughout G. A maximal flow in a weighted graph G maximises the

flow through the $t \rightarrow s$ edge. Ford and Fulkerson [7] demonstrated that the maximal s-t flow equals the minimum s-t cut, with the flow saturated uniformly on the cut.

Strang [21] and Iri [22] explored the extension of maximal flows to continuous domains. A continuous flow has the following properties:

- Conservation of flow: $\nabla \cdot \vec{F} = 0$.
- Capacity constraint: $\left|\vec{F}\right| \leq g$.

Let $\vec{F}$ be any flow and S be any simple, closed and smooth surface containing the source s. Let N_S denote the normal to the surface S and $\nabla \cdot \vec{F}_s$ the net flow out of the source s. Then, combining the two properties stated above, we obtain:

$$\nabla \cdot \vec{F}_s = \oint_S \vec{F} \cdot \vec{N}_S \mathrm{d}S \leq \oint_S g \mathrm{d}S. \tag{4}$$

Therefore, all flows are bounded from above by all smooth, simple and closed surfaces separating the source and sink, and vice versa. In fact, Strang showed that the maximal flow $\vec{F}_{\max}$ is strictly equal to the minimal surface $S_{\min}$ in the planar case while Iri explored the general case. For such a flow and surface, the flow saturates the surface uniformly:

$$\forall \vec{x} \in S_{\min}, \quad \vec{F}_{\max}(\vec{x}) = g(\vec{x}) \vec{N}(\vec{x}). \tag{5}$$

The minimal surface algorithm presented in this paper makes explicit use of this duality.

The duality between maximal flows and minimal cuts and surfaces has a simple interpretation. Any cut forms a bottleneck for a flow, limiting the flow to be less than the capacity of that cut. The maximal flow is limited by all possible cuts, and therefore must be less than or equal to the cost of the minimal cut. These dualities state that the maximal flow is indeed equal to the minimal cut, and therefore that a maximal flow saturates all edges belonging to a minimal cut.

D. Approximating minimal surfaces by graph cuts

A number of approaches have been proposed to compute approximate minimal surfaces by transforming the problem to a graph cut. These approaches obtain a polyhedral surface of minimal weighted area, where the weighting is derived from the metric of the original Riemannian space.

Hu presented a formulation of the minimum cut problem in a graph with vertex capacities rather than edge capacities [23]. Under this alternate formulation a cut becomes a set of vertices whose removal disconnects the source and sink. The cost of a cut is the sum of the capacities

of these vertices. The continuous problem is modelled as a grid of square vertices of sidelength h. The vertex capacities are sampled directly from the metric of the continuous domain. All vertices are connected within a radius $r \gg h$. Hu showed that, in the limit as $h \to 0$, $r \to 0$ and $\frac{h}{r} \to 0$ the minimum cut converges to a surface of minimal weighted area. Hu's method can only approximate isotropic metrics.

Boykov and Kolmogorov [24] present an approximation to the minimal surface problem using a graph with edge capacities derived from the metric of the continuous domain. Their approach is able to handle all convex metrics. Edge capacities are derived from the metric of the continuous domain using the Cauchy-Crofton formula from integral geometry.

In both of these approximations the theoretical convergence of a minimum cut to a minimal surface depends upon the degree of each vertex increasing toward infinity. In practice the number of directions that each segment of the polyhedral approximation can take on is proportional to the degree of each vertex. For an angular precision of $\Delta\theta$, the degree of each vertex is proportional to $(\frac{1}{\Delta\theta})^N$ in Hu's formulation and $(\frac{1}{\Delta\theta})^{N-1}$ in Kolmogorov's formulation. Consequently the time and memory required by these algorithms grows rapidly with the desired angular resolution, particularly in higher dimensions.

IV. The planar case

In the 2-D case some special equivalences exist between, on the one hand, minimal paths and geodesics, and on the other hand minimal cuts and surfaces. These equivalences require quite strict assumptions on the domain but when applicable they may be used to transform problems of one type to an equivalent problem of the other type. These dualities are important in the design of planar minimal cut algorithms because the computation of shortest paths is efficient, compared to more general maximal flow methods. They are used in Weihe's discrete maximal flow algorithm [25] and in Mitchell's continuous maximal flow algorithm [26].

A. Planar Spaces

Consider a graph G and a Riemannian space R as before. A graph is *planar* if it may be embedded in the plane $I\!R^2$ such that no edges cross. Likewise, a space R is planar if it is homotopically equivalent (may be deformed smoothly) to the plane $I\!R^2$. These embeddings

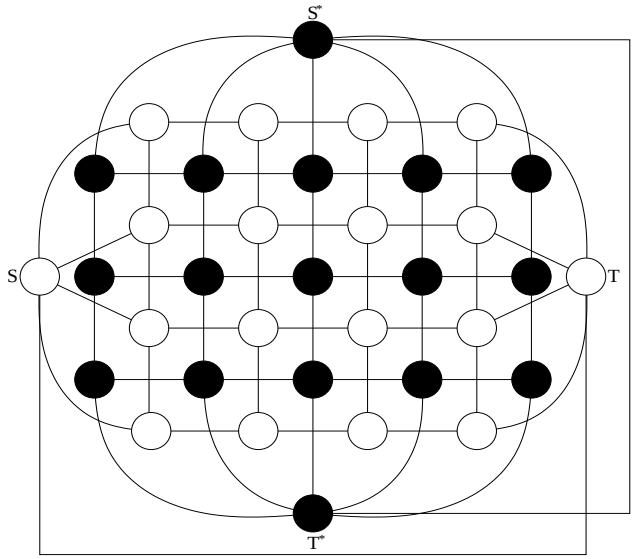

Fig. 1. A planar graph (white) and its dual (black).

must be performed with the $t \to s$ edge included, which further restricts the application of planar equivalences.

B. Planar Duals

For an edge-weighted graph G we define the *planar dual* graph G^*. Each dual vertex in G^* corresponds to a *face* in G. A face is an open region bounded by edges. A dual edge in G^* connects adjacent faces in G. An example of a planar graph and its dual is given in Figure 1. The planar dual of the planar dual is the identity: $G^{**} \equiv G$. The Riemannian spaces with isotropic metric that we consider here are self-dual: $R^* \equiv R$.

C. Discrete Path-Cut Dualities

Consider an s-t maximal flow in a weighted graph G. Let G be planar, and let s^*, t^* denote the dual vertices in G^* which are connected by the dual edge corresponding to $t \to s$. Following [25] we may derive an s-t maximal flow and corresponding minimal cut in G from the distance function and corresponding s^*-t^* shortest path in G^*:

1) Maximal flow — distance function duality: Let $D_G : V^* \to I\!R$ be the shortest distance from s^* to each vertex in V^*. Let $F_G : E \to I\!R$ be the flow in G. To all edges in G and G^* assign a direction arbitrarily. Then $F_G(e) = e \times e^* \Delta D_G(e^*)$ for dual edges $e \equiv e^*$. Here $\Delta D_G(e^*)$

denotes the directed difference between the distances at each endpoint of edge e^*, while $e \times e^*$ denotes the sign of the cross-product of the directions e by e^* in the planar embedding.

2) Minimal cut — shortest path duality: The edge set of an s-t minimal cut Γ_G in G corresponds exactly to the dual edges along an s^*-t^* shortest path in G^*.

D. Continuous Geodesic-Minimal Surface Dualities

In the continuous case consider an s-t maximal flow in a planar Riemannian space R. Let s^*, t^* be the dual source and sink vertices. Then we may derive an s-t maximal flow and corresponding minimal surface in R from the distance function and corresponding s^*-t^* shortest path in R^* as follows:

1) Maximal flow — distance function duality: Let D_R be the minimal distance from s^* to each point in R^*. Let $\vec{F}_R$ be the flow in R. Then $\vec{F}_R = \nabla^\perp D_R$ everywhere, where $\nabla^\perp D_R$ denotes the rotation by $-\frac{\pi}{2}$ of the gradient of D_R. Here the distance D_R corresponds to the vector potential of the flow $\vec{F}_R$. In the planar case it is known as the *stream function*, with $\vec{F}_R = \nabla \times \left(D_R \hat{\vec{k}} \right)$. $\hat{\vec{k}}$ is the unit vector pointing out of the plane Ω.

2) Minimal surface — geodesic duality: The s-t minimal surface and s^*-t^* geodesic are identical.

E. Minimal Cycles

The problem of obtaining minimal cycles or closed contours is more challenging than that of obtaining minimal paths and geodesics. The discrete case has been investigated by Sun and Pallottino [27] and Appleton and Sun [28]. The continuous case has been more recently studied by Appleton and Talbot [20] resulting in the Globally Optimal Geodesic Active Contour (GOGAC) algorithm.

V. Minimal surfaces in higher dimensions

Unfortunately the duality between minimal paths and minimal surfaces breaks down in higher dimensions, in part because they have different dimensions. Here we present an algorithm for obtaining continuous maximal flows in arbitrary spaces with scalar metric.

A. A continuous maximal flow algorithm

Consider the following system of partial differential equations:

$$\frac{\partial P}{\partial t} = -\nabla \cdot \vec{F} \tag{6}$$

$$\frac{\partial \vec{F}}{\partial t} = -\nabla P \tag{7}$$

subject to

$$\left|\vec{F}\right| \leq g \tag{8}$$

We relax the requirement that $\vec{F}$ have zero divergence (Section III-C) by introducing the potential field P which is conserved under the flow (Equation 6). Equation 7 introduces coupling such that gradients in the potential field P drive the flow $\vec{F}$. Equation 6 and 7 form a simple system of wave equations. They may be viewed as a linear model of the dynamics of an idealised fluid with pressure P and velocity $\vec{F}$, ignoring convection terms. Equation 8 constitutes a hard constraint on the magnitude of the flow velocity $\vec{F}$. It is unique to the maximal flow problem and does not appear to have an immediate physical analogy.

For boundary conditions we fix the scalar field P at the source s and sink t: $P_s = 1$ and $P_t = 0$. These values are chosen arbitrarily without loss of generality.

B. Properties of the continuous maximal flow algorithm

1) Conservation of potential P: Let $P_A = \int_A P \mathrm{d}A$ denote the total integral of P in a given region A not including s, t.

Then, for smooth P and $\vec{F}$,

$$\begin{aligned}
\frac{\partial P_A}{\partial t} &= \int_A \frac{\partial P}{\partial t} \mathrm{d}A \\
&= -\int_A \left(\nabla \cdot \vec{F}\right) \mathrm{d}A \\
&= -\oint_{\partial A} \vec{F} \cdot \vec{N}_{\partial A} \mathrm{d}\left(\partial A\right)
\end{aligned}$$

So P is conserved in the interior of any *sourceless* region A (any region not including the source s or sink t).

2) Monotonic reduction of energy $\frac{1}{2}(P^2 + \|\vec{F}\|_2^2)$*:* Consider the temporal rate of change of the total quantity of $\frac{1}{2}(P^2 + \left\|\vec{F}\right\|_2^2)$ in a given region A not including s, t. For smooth P and $\vec{F}$,

$$\begin{aligned}
\frac{\partial}{\partial t}\int_A \frac{1}{2}\left(P^2 + \vec{F}^2\right)\mathrm{d}A &= \int_A \frac{\partial}{\partial t}\frac{1}{2}\left(P^2 + \vec{F}^2\right)\mathrm{d}A \\
&= \int_A \left(\frac{\partial P}{\partial t}P + \frac{\partial \vec{F}}{\partial t}\cdot\vec{F}\right)\mathrm{d}A \\
&= -\int_A \left(P\left(\nabla\cdot\vec{F}\right) + (\nabla P)\cdot\vec{F}\right)\mathrm{d}A \\
&= -\oint_{\partial A} P\vec{F}\cdot\vec{N}_{\partial A}\mathrm{d}\left(\partial A\right)
\end{aligned}$$

Note that we have momentarily ignored the magnitude constraint (Equation 8). Consequently $\frac{1}{2}(P^2 + \|\vec{F}\|_2^2)$ is conserved in the interior of any sourceless region A. Including the magnitude constraint may only decrease $\|\vec{F}\|_2^2$ and hence the energy $\frac{1}{2}(P^2 + \|\vec{F}\|_2^2)$ must monotonically decrease in the interior of a sourceless region. Since the energy is positive it must converge. To ensure smoothness and convergence of P and $\vec{F}$ independently, a dissipative term can be added to the equations. In practice this term is not necessary.

C. Correctness at convergence

At convergence any isosurface of P may be taken as the globally minimal surface $S_{\min}$ separating s and t.

Proof: Setting temporal derivatives to zero at convergence, we may restate the system (Equations 6, 7, 8):

$$\nabla\cdot\vec{F} = 0$$

$$\begin{aligned}
\nabla P &= 0 && && \text{if } \left|\vec{F}\right| < g \\
\nabla P &= -\lambda\vec{F} && \text{where} \quad \lambda \geq 0 && \text{if } \left|\vec{F}\right| = g
\end{aligned}$$

The first equation simply restates the conservation of flow. The second equation is derived from Equations 7, 8. It states that where $\vec{F}$ is not saturated P must be constant, and where $\vec{F}$ is saturated ∇P must be such that $\vec{F}$ cannot change direction or decrease in magnitude. Consequently $\nabla P\cdot\vec{F} \leq 0$, indicating that P is a (non-strictly) monotonic function along the

flow lines of $\vec{F}$. As $\vec{F}$ is divergence-free, flow lines may only initiate at s and terminate at t. Therefore there are no local extrema in P.

Now consider the closed region A_p obtained from P by the application of a threshold $0 < p < 1$:

$$A_p = \{\vec{x} \,|P(\vec{x}) \geq p\}$$

Due to the monotonicity of P this region contains the source s. On the isosurface $S = \partial A_p$ we have $\nabla P \neq \vec{0}$ by construction. Therefore the flow is uniformly saturated outward on this surface and we obtain:

$$\nabla \cdot \vec{F}_s = \oint_S \vec{F} \cdot N_S \mathrm{d}S = \oint_S g \mathrm{d}S.$$

Hence $\vec{F}$ and S satisfy Equation 5 for optimality. Therefore at convergence any isosurface of P is a globally minimal surface. In the usual case of a unique minimal surface, $S_{\min}$ will be the only isosurface at convergence and hence P will approach an indicator function for the interior of $S_{\min}$. ■

D. Implementation

Equations 6, 7 are discretised on a staggered grid using an explicit first-order scheme in time and space. The scalar field P is stored on grid points while the vector field $\vec{F}$ is stored by component on grid edges, depicted in Figure 2. The system of equations is iterated sequentially with the flow magnitude constraint (Equation 8) enforced after each timestep.

Here for simplicity we describe the update scheme for a single iteration in 2 dimensions. The spatial grid step is set to $h = 1$. We first consider the linear portion of the update scheme, implementing Equations 6, 7. Let n denote the iteration number and Δt the timestep. The spatial grid step is set at $h = 1$. Let $P^n_{i,j}$ denote the value of the potential at time $n\Delta t$ and grid point (i, j) and let $g_{i,j}$ denote the value of the metric at the point (i, j). Let $F^n_{i\pm\frac{1}{2},j,x}$ and $F^n_{i,j\pm\frac{1}{2},y}$ represent the components of the flow along the four edges incident on the point (i, j) at time $n\Delta t$.

$$P^{n+1}_{i,j} = P^n_{i,j} - \Delta t \left(\left(F^n_{i+\frac{1}{2},j,x} - F^n_{i-\frac{1}{2},j,x} \right) + \left(F^n_{i,j+\frac{1}{2},y} - F^n_{i,j-\frac{1}{2},y} \right) \right) \tag{9}$$

$$\begin{aligned} F'^{n+1}_{i+\frac{1}{2},j,x} &= F^n_{i+\frac{1}{2},j,x} - \Delta t \left(P^n_{i+1,j} - P^n_{i,j} \right) \\ F'^{n+1}_{i,j+\frac{1}{2},y} &= F^n_{i,j+\frac{1}{2},y} - \Delta t \left(P^n_{i,j+1} - P^n_{i,j} \right) \end{aligned} \tag{10}$$

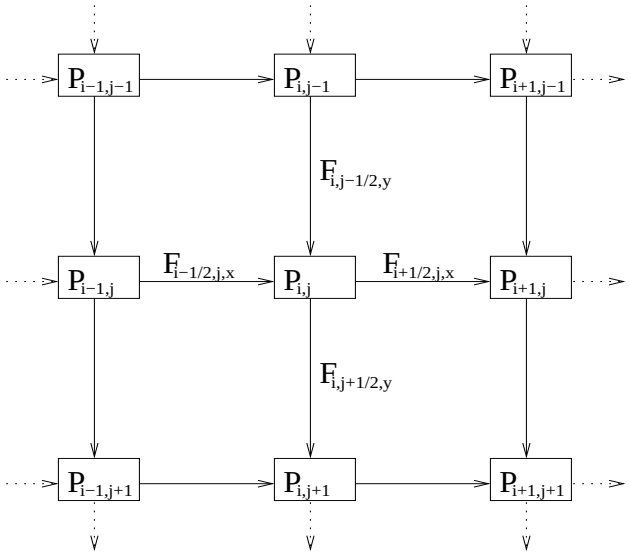

Fig. 2. Grid structure underlying the numerical scheme presented here. P is stored on grid points while $\vec{F}$ is stored by component on grid edges.

The magnitude constraint is applied immediately following the update of the flow velocity field by Equation 10. Here we describe the application of the magnitude constraint at point (i, j) for time $(n + 1)\Delta t$, consisting of three stages:

1) Determine the maximum outward flow along each axis:

$$\begin{aligned} \left|F^{n+1}_{i,j,x}\right|' &= \max\left(-F'^{n+1}_{i-\frac{1}{2},j,x},\ 0,\ F'^{n+1}_{i+\frac{1}{2},j,x}\right) \\ \left|F^{n+1}_{i,j,y}\right|' &= \max\left(-F'^{n+1}_{i,j-\frac{1}{2},y},\ 0,\ F'^{n+1}_{i,j+\frac{1}{2},y}\right) \end{aligned}$$

2) Compare the absolute maximum outward velocity to the metric $g_{i,j}$:
If $v'^{n+1}_{i,j} \equiv \sqrt{\left(\left|F^{n+1}_{i,j,x}\right|'\right)^2 + \left(\left|F^{n+1}_{i,j,y}\right|'\right)^2} > g_{i,j}$ then

$$\begin{aligned} |F^{n+1}_{i,j,x}| &= |F^{n+1}_{i,j,x}|' \frac{g_{i,j}}{v'^{n+1}_{i,j}} \\ |F^{n+1}_{i,j,y}| &= |F^{n+1}_{i,j,y}|' \frac{g_{i,j}}{v'^{n+1}_{i,j}} \end{aligned}$$

3) Apply the magnitude constraint to each outward velocity component:

$$\begin{aligned} F^{n+1}_{i-\frac{1}{2},j,x} &= \max\left(F'^{n+1}_{i-\frac{1}{2},j,x},\ -|F^{n+1}_{i,j,x}|\right) \\ F^{n+1}_{i+\frac{1}{2},j,x} &= \min\left(F'^{n+1}_{i+\frac{1}{2},j,x},\ |F^{n+1}_{i,j,x}|\right) \end{aligned}$$

$$F^{n+1}_{i,j-\frac{1}{2},y} = \max\left(F'^{n+1}_{i,j-\frac{1}{2},y},\ -|F^{n+1}_{i,j,y}|\right)$$
$$F^{n+1}_{i,j+\frac{1}{2},y} = \min\left(F'^{n+1}_{i,j+\frac{1}{2},y},\ |F^{n+1}_{i,j,y}|\right)$$

Despite the complexity of its formal description, this update scheme is simple enough that a single implementation is used to handle input data of arbitrary dimension.

Several heuristics have been found to increase the speed of convergence. The fields P and $\vec{F}$ are rapidly initialised using the pre-flow push discrete maximal flow algorithm of Goldberg and Tarjan with both global and gap relabelling [15]. A multiscale approach is also applied recursively for rapid convergence at a fine grid resolution from a coarse grid estimate. Computation may be avoided in the interior of the source s and sink t, yielding great savings when they occupy a significant portion of the space.

At convergence, in the usual case of a unique surface of globally minimal value, the potential field P is theoretically perfectly binary with value 1 within the volume bounded by the minimal surface, and 0 outside. In practice convergence is deemed to be attained if the sum of the relative areas of potential $|A_{P\geq 1-\gamma}|$ and $|A_{P\leq\gamma}|$ is greater than $\mu\%$. For example, $\gamma = 0.03$ and $\mu = 99$.

E. Stability

In this section we derive the maximum timestep for which the update scheme described by Equations 9, 10 is stable. In this analysis we neglect the magnitude constraint as it may only reduce the magnitudes of the variables of interest and hence cause the system to tend toward stability. For simplicity we perform the derivation in the 2-dimensional case and then give the general solution.

By an appropriate combination of Equations 9, 10 we may obtain the discrete update equation solely for P:

$$P^{n+2}_{i,j} - 2P^{n+1}_{i,j} + P^{n}_{i,j} = (\Delta t)^2\left(-4P^{n}_{i,j} + P^{n}_{i+1,j} + P^{n}_{i-1,j} + P^{n}_{i,j+1} + P^{n}_{i,j-1}\right) \tag{11}$$

This is a discrete analogue to the wave equation

$$\frac{\partial^2 P}{\partial t^2} = \nabla^2 P \tag{12}$$

which may be derived from Equations 6, 7.

Equation 11 describes a linear system and so is amenable to spectral analysis. Specifically, consider the Z-transform over $z_x,\ z_y,\ z_t \in \mathbb{C}$ with $|z_x| = |z_y| = 1$ for a bounded field P:

$$P(z_x, z_y, z_t) = \sum_{i,j,n} P^n_{i,j} z_x^i z_y^j z_t^n \tag{13}$$

For $P \neq 0$ substitution into Equation 11 gives

$$\begin{aligned} P(z_x, z_y, z_t)\left(z_t^2 - 2z_t + 1\right) &= P(z_x, z_y, z_t)(\Delta t)^2\left(-4 + z_x + z_x^{-1} + z_y + z_y^{-1}\right) \\ \therefore \left(z_t^2 - 2z_t + 1\right) &= (\Delta t)^2\left(-4 + z_x + z_x^{-1} + z_y + z_y^{-1}\right) \end{aligned} \tag{14}$$

For a system on the border of stability $|z_t| = 1$. Now the right side of Equation 14 ranges in value from 0 to $-8(\Delta t)^2$ over the entire spatial spectrum. The left side ranges in value from 0 to -4. In order that this equation have a solution for all spatial frequency components, we require that it have a solution when the right side equals $-8(\Delta t)^2$, *i.e.*

$$\begin{aligned} -4 &\leq -8(\Delta t)^2 \\ \therefore \Delta t &\leq \frac{1}{\sqrt{2}} \end{aligned}$$

More generally when the update is performed in N dimensions it is simple to show that $\Delta t \leq \frac{1}{\sqrt{N}}$.

This result coincides with the Courant-Friedrich-Lévy stability condition, a necessary condition for numerical stability. This states that information must propagate through the numerical grid at least as fast as information propagates in the PDE that it models. Consider the continuous wave equation for P (Equation 12) and consider the spectral component $P = e^{(t\omega_t + x\omega_x + y\omega_y + \ldots)\sqrt{-1}}$. Substituting this into Equation 12 gives

$$\begin{aligned} P\omega_t^2 &= P\left(\omega_x^2 + \omega_y^2 + \ldots\right) \\ \therefore \omega_t &= \pm\sqrt{\omega_x^2 + \omega_y^2 + \ldots} \end{aligned}$$

Therefore the physical wave velocity $v = \left|\frac{\omega_t}{\sqrt{\omega_x^2 + \omega_y^2 + \ldots}}\right| = 1$ for all spatial frequencies. As physical waves travel at unit speed in grid coordinates, the timestep in the update scheme must be such that information may travel through the grid at least as fast. For the scheme described in Equations 9, 10, information travels along one edge per timestep. Therefore in N dimensions this scheme requires N timesteps to travel in the 'diagonal' direction described by the unit vector $(1, 1, \ldots)$ of length $\sqrt{N}$. So, $N\Delta t < \sqrt{N}$ and hence $\Delta t < \frac{1}{\sqrt{N}}$ as before.

VI. Metric weighting functions

Minimal surface methods have an inherent bias in favour of small surfaces. In many applications this is undesirable, resulting in incorrect or even trivial solutions. In this section we present a technique to automatically remove this bias.

Consider a metric that is uniformly constant throughout the domain, $g = 1$. This metric conveys no preference for any particular point through which the partition surface should pass. Intuitively then, every point in the domain should belong to some (globally) minimal surface. Unfortunately as the minimal surface problem is posed this is not the case. In order to improve the behaviour of the solutions to this problem then, we replace the metric g by $g' = gw$, introducing an appropriate weighting function w. This weighting function will account for the geometry of the sources and sinks, so that the minimal surface depends only on the data as represented by g.

Appleton and Talbot considered the case of a single point source $\mathbf{p}$ in a planar image [20]. Here it was demonstrated that the introduction of the weighting function $w(\mathbf{x}) = \frac{1}{|\mathbf{x}-\mathbf{p}|}$ resulted in a continuum of minimal surfaces, the set of all circles centred on $\mathbf{p}$. In N dimensions it is simple to see that the modified weighting function $w(\mathbf{x}) = \frac{1}{|\mathbf{x}-\mathbf{p}|^{N-1}}$ will behave similarly, ensuring that each point in the domain belongs to a minimal surface (a hypersphere centred on $\mathbf{p}$). These weighting functions may be extended to other seed geometries. For a line source in 3 dimensions we obtain the weighting function $w(\mathbf{x}) = \frac{1}{|\mathbf{x}-\mathbf{p}|}$ where $\mathbf{p}$ is the nearest point to $\mathbf{x}$ on the line. More generally for a set of seeds which form an M-dimensional manifold embedded in N dimensions we should expect a weighting function that decays as $\frac{1}{|\mathbf{x}-\mathbf{p}|^{N-M-1}}$ in the neighbourhood of the manifold.

We wish to derive an *unbiased* flow $\vec{F}$ from which we may define the weighting function $w = |\vec{F}|$. This flow will be produced by the source set s and absorbed by the sink set t,

$$\nabla \cdot \vec{F} = \rho \tag{15}$$

where ρ is a distribution that is zero in the interior of the domain, positive on the source set s and negative on the sink set t, with total source weight $\int_s \rho \mathrm{d}V = 1$ and sink weight $\int_t \rho \mathrm{d}V = -1$. There will naturally be many such flows; here we select a flow to minimise a measure of the weighting function

$$E[w] = \int_V \frac{1}{2} w^2 \mathrm{d}V = \int_V \frac{1}{2} \vec{F}^2 \mathrm{d}V.$$

In this way we will ensure that the weighting function is not arbitrarily large at any particular point in space, as it could be for example for some flows with large rotational components.

We may minimise the measure $E[\vec{F}] \equiv E[w]$ by variational calculus: consider adding a minimisation parameter t to obtain $w \equiv w(\vec{x}, t)$. Then we may compute the first variation with respect to t to determine the local minima of $E[\vec{F}]$:

$$\frac{\delta E[\vec{F}]}{\delta t} = \int_V \vec{F}_t \cdot \vec{F} \mathrm{d}V = 0$$

Here we have set the first variation to 0 to obtain a local minimum condition on $E[w]$. This minimisation must be carried out subject to the incompressibility constraint introduced in Equation 15. Therefore a flow $\vec{F}$ which satisfies Equation 15, the flow must still satisfy this constraint a short time time later. So we obtain equivalent constraints on $\vec{F}_t$:

$$\nabla \cdot \vec{F}_t = 0$$

Therefore $\vec{F}_t$ may be decomposed into cyclic components, and $\vec{F}$ is a local minimum of $E[\vec{F}]$ if it is locally minimal with respect to all cyclic flows. Consider then $\vec{F}_t = \vec{T}_C$ the unit tangent vector over some cyclic curve C, with $\vec{F}_t = 0$ elsewhere. For $\vec{F}$ a local minimum of $E[\vec{F}]$ we have

$$\begin{aligned} \frac{\delta E[\vec{F}]}{\delta t} &= \int_V \vec{F}_t \cdot \vec{F} \mathrm{d}V \\ &= \int_C \vec{F}_t \cdot \vec{T}_C \mathrm{d}C \\ &= 0 \end{aligned}$$

So we find that the vector field is a potential flow. Set $\vec{F}_t = \nabla \phi_t$ then, and replace the divergence of the flow $\vec{F}$ in Equation 15 by the Laplacian of ϕ to obtain

$$\nabla^2 \phi = \rho$$

We choose boundary conditions $\lim_{|\mathbf{x}| \to \infty} \nabla \phi(\mathbf{x}) = 0$ so that the flow is zero at infinity. ϕ is then determined up to the addition of a constant which will not affect the weighting function $w = |\nabla \phi|$.

Observe now that all isosurfaces S of ϕ in the interior of the domain have constant net flux $\int_S \nabla \phi \cdot \vec{N}_S \mathrm{d}S = 1$. As $w = |\nabla \phi|$ we then obtain $\int_S w \mathrm{d}S = 1$ over all isosurfaces of ϕ, with $\int_S w \mathrm{d}S \geq 1$ for all closed surfaces S containing the seeds. So the isosurfaces of ϕ form the

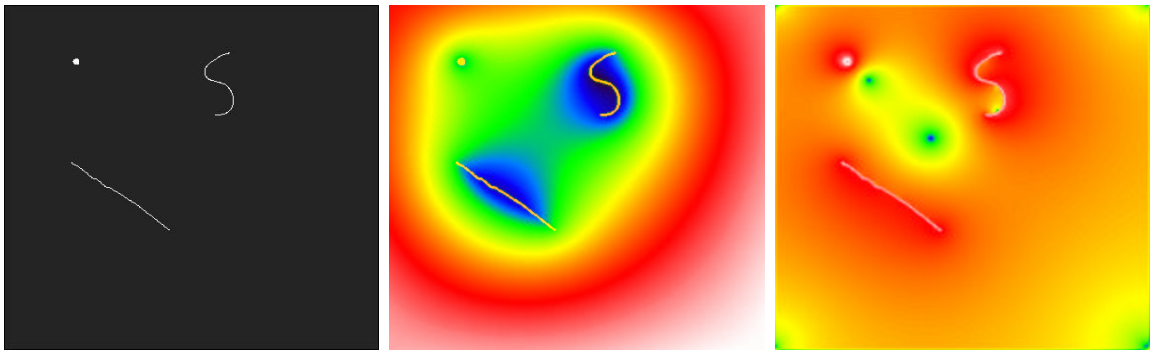

(a) (b) (c)

Fig. 3. Metric weighting example. (a) The seed geometry. Source points are depicted, while the sink points are the image boundary. (b) Isosurfaces of the function ϕ computed by convolution. (c) The metric weighting w, computed from the numerical derivative of ϕ.

set of minimal surfaces under the metric w. In general we have $\nabla\phi \neq 0$ almost everywhere, therefore almost every point in the domain belongs to some minimal weighted surface under the metric w as desired.

A. Implementation

For the regular grids considered in this paper the weighting functions may be computed by convolving the distribution ρ with the *impulse response* $\phi_\odot$ which is the solution to $\nabla^2\phi_\odot = \delta(\mathbf{x})$. In 2 dimensions this is $\phi_\odot = \frac{1}{2\pi}\ln(r)$ while in 3 dimensions this is $\phi_\odot = -\frac{1}{4\pi r}$. This convolution may be efficiently computed using the Fast Fourier Transform. The gradient of ϕ may then be numerically estimated in the discrete grid to obtain the weighting function w.

Figure 3 shows an example of a set of seed points and the process of computing an appropriate weighting function. The weighting function is highest in the neighbourhood of point sources and the endpoints of line sources.

VII. Applications

In this section we present results for the application of minimal surfaces to the segmentation of 2D and 3D medical images and 3D reconstruction from stereo images.

All tests were performed on a 700MHz Toshiba P-III laptop with 192MB of RAM under the Linux operating system. The algorithm presented here has been implemented in C and has not been optimised significantly.

A. 2D Image Segmentation

Object boundaries are often difficult to detect along transitions to adjacent objects with similar features. Segmentation via minimal contours uses the regularisation of the segmentation contour to avoid leaking across such gaps. The authors have previously developed an algorithm, Globally Optimal Geodesic Active Contours (GOGAC), which efficiently computes globally minimal contours in planar Riemannian spaces [20]. Here we apply discrete minimal cuts, GOGAC, and the algorithm presented in this paper to segment a microscope image of a cluster of cells (Figure 4(a)) and compare the results.

We compute a metric (Figure 4(b)) from the microscope image as described in Equation 2, with default parameters $p = 1$ and $\varepsilon = 0$ and with blurring at scale $\sigma = 1$. Low metric regions are dark while high metric regions are bright. Observe that the regions of low metric correspond to the boundaries of the cells, except where the cells overlap.

Here we apply discrete minimal cuts, GOGAC [20], and the algorithm presented in this paper to segment a microscope image of a cluster of cells (Figure 4(a)) and compare the results. In spite of its apparent simplicity this problem outlines the challenge of delineating faint boundaries between cells without leaking.

The segmentation of each cell is performed independently in sequence. The source sets are depicted in (Figure 4(b-d)) while the sink is the image boundary. The discrete minimal cut solves a discretised minimal surface problem, resulting in a clear grid bias and a poor segmentation. GOGAC and the continuous maximal flow algorithm solve the same continuous optimisation problem and are in clear agreement. Note that the continuous segmentations follow the perceived cell contours even in the absence of local cues.

The image depicted in Figure 4(a) has dimensions 231×221. We reduce the amount of computation required by expanding the sink to include only the cells of interest, a region of size 150×100.

The discrete minimal cuts required 12.9 seconds to compute in total. GOGAC required 1.5 seconds to compute in total. The continuous minimal surface algorithm presented here required

5.1 seconds in total to converge.

B. 3D Image Segmentation

We apply the algorithm proposed in this paper to segment the lungs in the Computed Tomography image of a chest depicted in Figure 5, and compare this to a segmentation using Geodesic Active Surfaces and discrete minimal cuts. The same metric is used for all segmentations. For the cut methods the sources are small spheres inside each lung and the sink is the boundary of the volume, not including the uppermost face. The Geodesic Active Surfaces are initialised as spheres inside each lung, with an inflation term driving the surface to fill the lung. The two lungs are segmented separately in sequence.

The Geodesic Active Surfaces give an inaccurate segmentation (Figure 5(b)). At the base of the lung the inflation term is too weak for the surface to completely fill the lung, becoming trapped on edges due to alveoli. At the top of the lung the inflation term is too strong, causing the surface to leak through the weak edges of the lung.

Observe the directional bias along the grid in the discrete minimal cut. This is particularly evident at the flat boundaries in the interior surfaces at the top of the lungs (Figure 5(c)). By contrast, the continuous minimal surface does not exhibit such directional bias, giving a faithful segmentation (Figure 5(d)).

The data shown in Figure 5 has dimensions $200 \times 160 \times 90$. The Geodesic Active Surfaces required 22 minutes to converge to the final result. The discrete minimal cuts required 14 minutes to compute using Goldberg and Tarjan's pre-flow push algorithm to compute a maximal flow [15]. The continuous minimal surface algorithm required 8.5 minutes to converge, including all initialisation.

C. 3D Scene Reconstruction from Stereo Images

We apply our maximal flow algorithm to the reconstruction of a scene from a stereo image pair. The metric used here is based on the Zero-mean Normalised Cross Correlation (ZNCC) area based matching score, popular for its good statistical basis and efficient computation [12]. Here ZNCC scores are computed using a window of size 5×5. Scores are computed for integer disparities in the range $[-15, 0]$. We set $g = 1 - ZNCC$ throughout the disparity volume to

convert the problem of finding a maximal surface into that of finding a minimal surface. Following Roy and Cox [13] the source and sink are the first and last disparity layer respectively.

Figure 6 depicts the results of the reconstructions using both a discrete and a continuous minimal cut. Both disparity maps and the corresponding surfaces are shown. The results computed from the discrete minimal cut show very distinct flat zones due to the small number of disparities considered, while the continuous minimal surface is able to capture detail below the discrete level. As a result additional features are visible in the continuous minimal surface, including the third parking meter and the large scale surface texture of the bushes. Observe the absence of bias in the shape of the frame of the car.

The stereo image pair used here has dimensions 256×240. The discrete minimal cut required 230 seconds to compute. The continuous minimal surface algorithm required 140 seconds to converge including initialisation.

VIII. Conclusions

In this paper we have described a novel algorithm to compute continuous maximal flows in Riemannian spaces with scalar metric.

We have modelled this flow using a system of PDEs simulating the flow of an ideal fluid with spatially varying velocity constraints. The computation is implemented by a first order finite differences scheme. For efficiency reasons a discrete maximal flow result is used for initialization and a multi-resolution scheme is also used. In spite of this the total computational cost is significant, especially in 3-D at high resolution.

At convergence, the solution exhibits globally maximal flow, trivially yielding the expected minimal surface. However a full proof of convergence is not given in this paper and requires more work.

The new algorithm has been applied to segmentation in 2D and 3D medical images and to 3D reconstruction from a stereo image pair. The results in 2D agreed remarkably well with an existing planar minimal surface algorithm. The results in 3D segmentation and reconstruction demonstrated that, in constrast to existing discrete optimisation algorithms, the new algorithm computes surfaces which are not biased by the choice of computational grid. We believe these benefits may outweigh the computational cost of the method in cases where accuracy is paramount. The proposed algorithm also provides an accuracy benchmark for fast approximate methods.

ACKNOWLEDGEMENTS

We would like to acknowledge Simon Long of the University of Queensland for an interesting discussion leading to the numerical implementation of the metric weighting scheme presented in this paper.

REFERENCES

[1] M. Kass, A. Witkin, and D. Terzopoulos, "Snakes: Active contour models," *International Journal of Computer Vision*, vol. 1, no. 4, pp. 321–331, 1998.

[2] S. Osher and J. A. Sethian, "Fronts propagating with curvature-dependent speed: Algorithms based on Hamilton-Jacobi formulations," *Journal of Computational Physics*, vol. 79, pp. 12–49, 1988. [Online]. Available: citeseer.nj.nec.com/osher88fronts.html

[3] J. A. Sethian, *Level Set Methods and Fast Marching Methods - Evolving Interfaces in Computational Geometry, Fluid Mechanics, Computer Vision, and Materials Science*. Cambridge University Press, 1999.

[4] V. Caselles, R. Kimmel, and G. Sapiro, "Geodesic active contours," *IJCV*, vol. 22, no. 1, pp. 61–79, 1997.

[5] V. Caselles, R. Kimmel, G. Sapiro, and C. Sbert, "Minimal surfaces based object segmentation," *IEEE Trans. on PAMI*, vol. 19, pp. 394–398, 1997.

[6] E. Dijkstra, "A note on two problems in connexion with graphs," *Numerische Mathematik*, vol. 1, pp. 269–271, 1959.

[7] J. L. R. Ford and D. R. Fulkerson, *Flows in Networks*. Princeton University Press, Princeton, NJ, 1962.

[8] L. D. Cohen, "On active contour models and balloons," *Computer Vision, Graphics, and Image Processing. Image Understanding*, vol. 53, no. 2, pp. 211–218, 1991. [Online]. Available: citeseer.nj.nec.com/cohen91active.html

[9] C. Xu and J. L. Prince, "Snakes, shapes and gradient vector flow," *IEEE Transaction on Image Processing*, vol. 7, no. 3, pp. 359–369, March 1998.

[10] Y. Ohta and T. Kanade, "Stereo by intra- and inter-scanline search using dynamic programming," *IEEE Trans. Pattern Anal. Mach. Intell.*, vol. 7(2), pp. 139–154, March 1985.

[11] S. Lloyd, "Stereo matching using intra- and inter-row dynamic programming," *Pattern Recognition Letters*, vol. 4, pp. 273–277, September 1986.

[12] C. Sun, "Fast stereo matching using rectangular subregioning and 3D maximum-surface techniques," *International Journal of Computer Vision*, vol. 47, no. 1/2/3, pp. 99–117, May 2002.

[13] S. Roy and I. J. Cox, "A maximum-flow formulation of the n-camera stereo correspondence problem," in *Int. Conf. on Computer Vision (ICCV'98)*, Bombay, India, January 1998, pp. 492–499.

[14] P. Bamford and B. Lovell, "Unsupervised cell nucleus segmentation with active contours," *Signal Processing (Special Issue: Deformable models and techniques for image and signal processing)*, vol. 71, no. 2, pp. 203–213, 1998.

[15] R. Sedgewick, *Algorithms in C*, 3rd ed. Addison-Wesley, 2002, no. 5.

[16] J. N. Tsitsiklis, "Efficient algorithms for globally optimal trajectories," *IEEE Transactions on Automatic Control*, vol. 40, no. 9, pp. 1528–1538, September 1995.

[17] J. Sethian, "A fast marching level set method for monotonically advancing fronts," in *Proceedings of the National Academy of Sciences*, vol. 93(4), 1996, pp. 1591–1595. [Online]. Available: citeseer.nj.nec.com/sethian95fast.html

[18] R. Goldenberg, R. Kimmel, E. Rivlin, and M. Rudzsky, "Fast geodesic active contours," *IEEE Trans. On Image Processing*, vol. 10, no. 10, pp. 1467–1475, 2001.

[19] L. D. Cohen and R. Kimmel, “Global minimum for active contour models: A minimal path approach,” *International Journal of Computer Vision*, vol. 24, no. 1, pp. 57–78, August 1997. [Online]. Available: citeseer.nj.nec.com/cohen97global.html

[20] B. Appleton and H. Talbot, “Globally optimal geodesic active contours,” *Journal of Mathematical Imaging and Vision*, 2002, accepted.

[21] G. Strang, “Maximal flow through a domain,” *Mathematical Programming*, vol. 26, pp. 123–143, 1983.

[22] M. Iri, *Survey of Mathematical Programming*. North-Holland, Amsterdam, 1979.

[23] T. C. Hu, *Integer Programming and Network Flows*. Addison-Wesley, Reading, MA, 1969.

[24] Y. Boykov and V. Kolmogorov, “Computing geodesics and minimal surfaces via graph cuts,” in *International Conference on Computer Vision*, Nice, France, October 2003, pp. 26–33.

[25] K. Weihe, “Maximum (s, t)-flows in planar networks in $O(|V|\log|V|)$ time,” *Journal of Computer and System Sciences*, vol. 55, no. 3, pp. 454–475, December 1997.

[26] J. S. Mitchell, “On maximum flows in polyhedral domains,” in *Proc. 4th annual symposium on computational geometry*, Urbana-Champange, Illinois, United States, 1988, pp. 341–351.

[27] C. Sun and S. Pallottino, “Circular shortest path in images,” *Pattern Recognition*, vol. 36, no. 3, pp. 709–719, March 2003.

[28] B. Appleton and C. Sun, “Circular shortest paths by branch and bound,” *Pattern Recognition*, vol. 36, no. 11, pp. 2513–2520, November 2003.

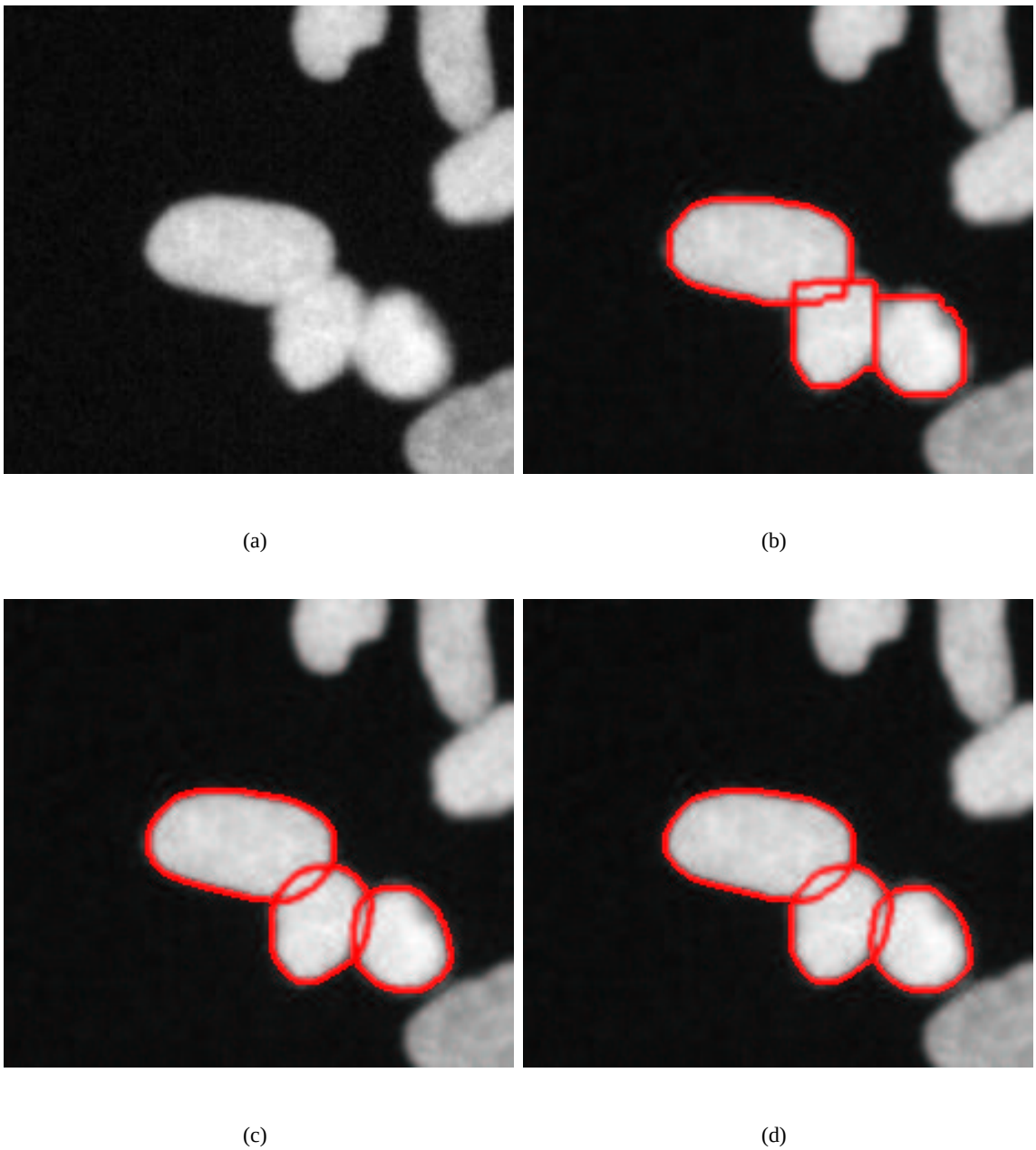

(a) (b)

(c) (d)

Fig. 4. Segmentation of a microscope image of a cell cluster. (a) The microscope image. (b) Segmentation via a discrete minimal cut. (c) Segmentation via Globally Optimal Geodesic Active Contours. (d) Segmentation via continuous maximal flows.

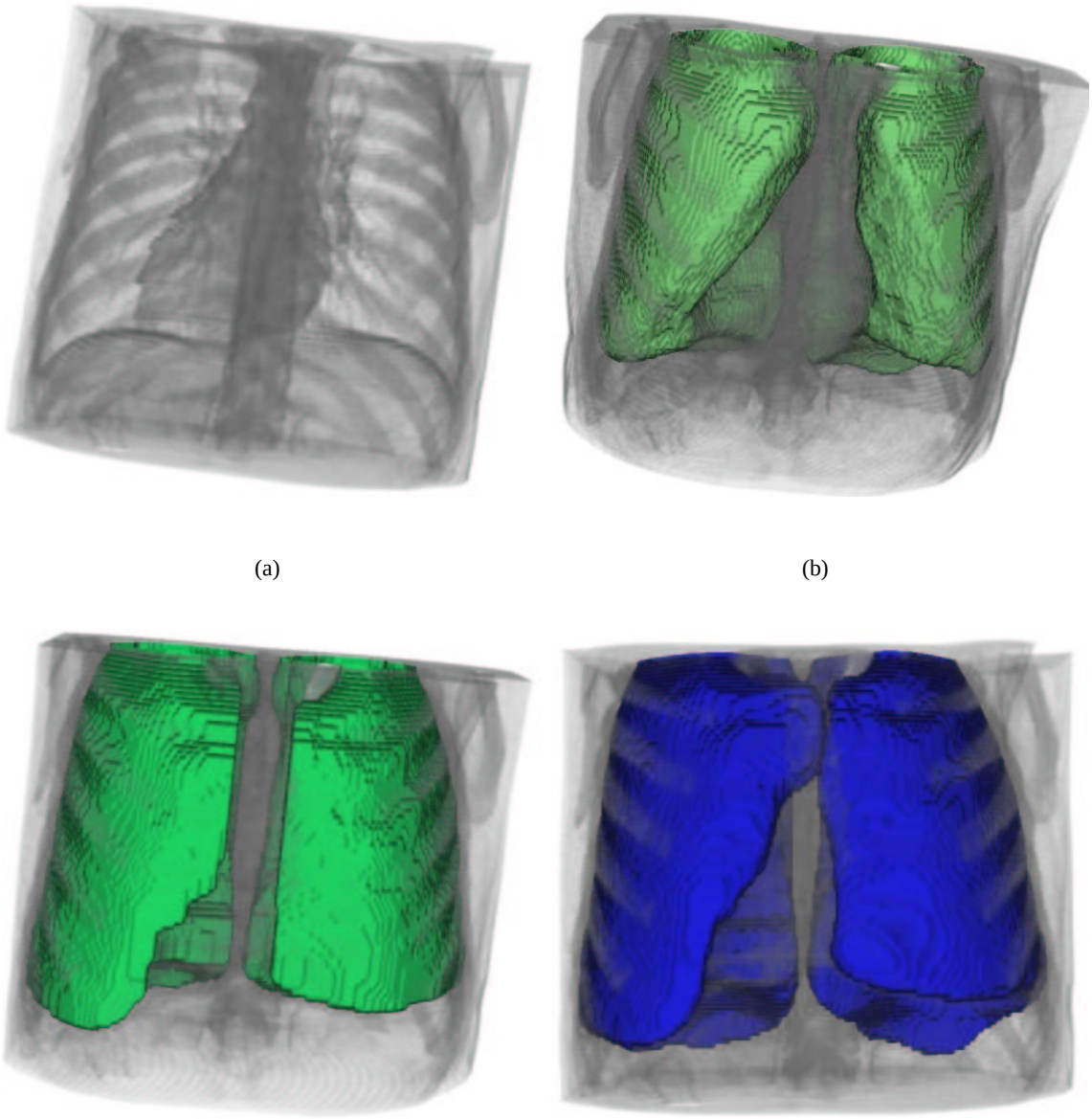

(a) (b)

(c) (d)

Fig. 5. Segmentation of the lungs in a chest CT image. (a) The CT image. (b) Segmentation using Geodesic Active Surfaces. The surfaces fail to fill the base of the lung. (c) Segmentation using a discrete maximal flow algorithm. Observe the directional bias due to the grid. (d) Segmentation from identical input using continuous maximal flows.

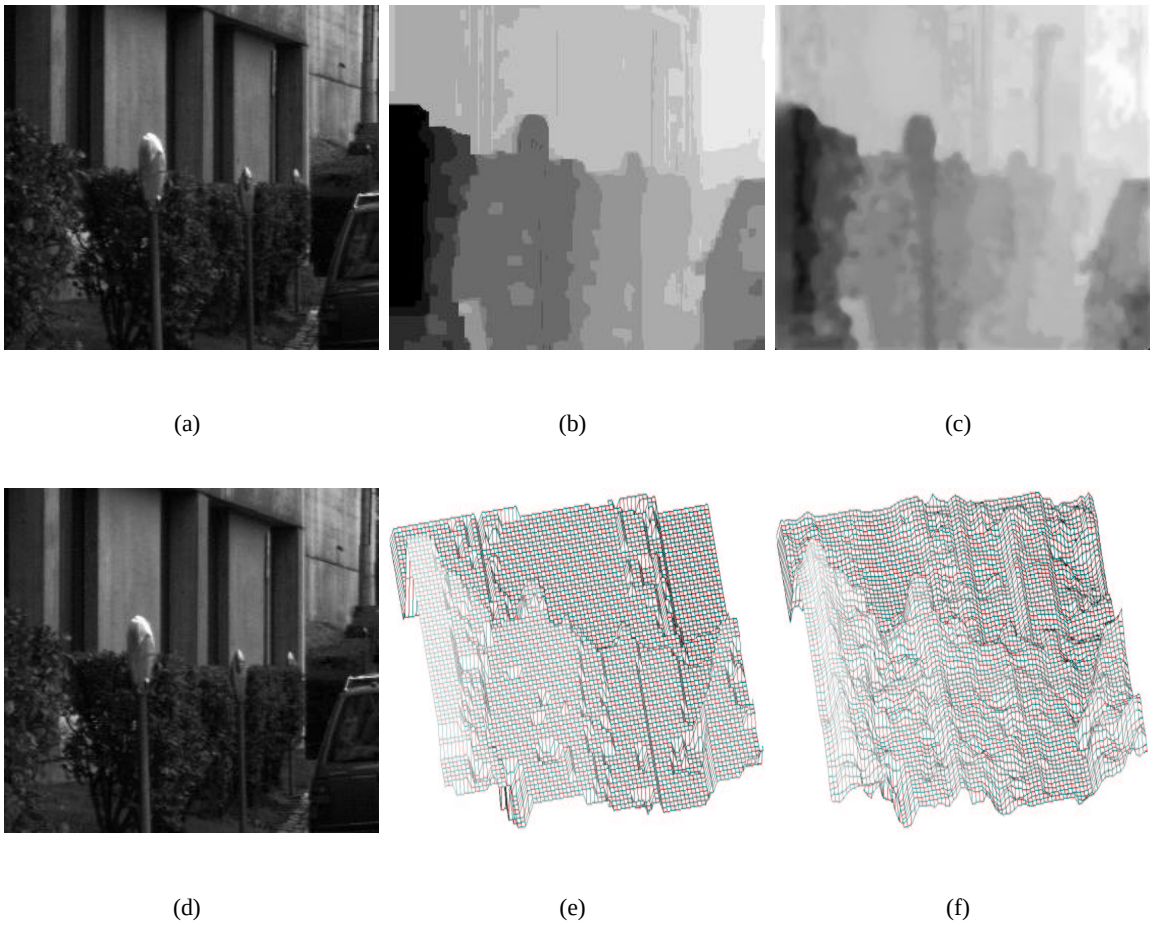

(a) (b) (c)

(d) (e) (f)

Fig. 6. Reconstruction of a scene from two views. (a, d) The two views. (b, e) Reconstruction (disparity map and mesh) from a discrete maximal flow. (c, f) Reconstruction from identical input using continuous maximal flows. Observe the additional detail.